Analysis of Precision Surface Grinding Using a Self-Assembled Dual-Optical-Fiber Real-Time Measurement System

Yu-Ting Lyu*, Ching-Yuan Chang*, Che-Wei Tu***, Chien-Ching Ma***, Yu-Chun Huang****, Herchang Ay*, Yu-Fu Lin****, Zheng-Han Hong**** and Po-Han Tseng*****

Keywords: Dual-fiber real-time measurement system, Internal residual stress, Grinding process.

ABSTRACT

This study applied a dual-optical-fiber real-time measurement system to precision surface grinding of FC-300 gray cast iron, focusing on internal strain and temperature variations. The system uses attached and free fibers to measure force- and heat-induced strains, respectively, with decoupling achieved through wavelength shift theory. In 14 grinding trials, the maximum temperature-induced strain reached 500 μe for workpiece A-2 and 1200 μe for workpiece B-2, while force-induced compressive strains peaked at -400 μe and -615.63 μe , respectively. These findings demonstrate the system's accuracy in capturing real-time strain variations, optimizing machining processes, and its potential for industrial applications.

Paper Received November, 2024. Revised February, 2025. Accepted February, 2025. Author for Correspondence: Herchang Ay,

- * Department of Mold and Die Engineering, National Kaohsiung University of Science and Technology, Kaohsiung, Taiwan
- ** Department of Mechanical Engineering, National Taipei University of Technology, Taipei, Taiwan
- *** Department of Mechanical Engineering, National Taiwan University, Taipei, Taiwan
- **** Department of Electrical Engineering, Southern Taiwan University of Science and Technology, Tainan, Taiwan
- ***** Metal Industries Research and Development Centre (MIRDC), Kaohsiung, Taiwan
- ****** Department of Mechanical Engineering, National Kaohsiung University of Science and Technology, Kaohsiung, Taiwan

INTRODUCTION

The grinding process is a critical step in modern manufacturing, where the removal of material layers through high-energy input leads to significant heat generation in the grinding zone. This localized heat concentration, resulting from the interaction between the grinding wheel and workpiece, causes uneven temperature distributions, leading to solid-phase transformations (Shuto et al., 2004; Sanchez-Pérez et al., 2025). The rapid heating and cooling cycles inherent in grinding processes can induce residual stresses, material cracking, and chemical alterations, which ultimately affect the mechanical properties of the workpiece, such as hardness and tensile strength (Breidenstein et al., 2024; Li et al., 2024).

In particular, phase transformations in gray cast iron result in plastic deformation, volume changes, and modifications to the material's internal structure (Zhang et al., 2021). Existing models primarily focus on predicting temperature evolution during the grinding process but often overlook the complex between thermal gradients mechanical deformation caused by grinding forces (Hadad and Sadeghi et al., 2012; Grigoriev et al., 2014). A comprehensive thermal-mechanical analysis is necessary to understand how these factors influence surface integrity, phase transformations, and the development of residual stresses (Qian et al., 2024; Gostimirovic et al., 2022).

Traditional methods for measuring residual stress, such as the hole-drilling technique or X-ray diffraction, while effective, are often destructive, costly, and unsuitable for real-time monitoring (Storchak et al., 2024). To overcome these limitations, this study presents a novel dual optical fiber real-time measurement system that allows for non-destructive,

real-time monitoring of thermal stresses and residual strains within the workpiece during grinding.

This system utilizes embedded optical fibers to enable direct measurement of thermal expansion and mechanical deformation. By using fiber Bragg gratings, the system decouples force-induced and temperature-induced strains, providing a more accurate and efficient method for optimizing grinding processes (Rowe et al., 2014; Lyu et al., 2024). Unlike conventional techniques, the dual-fiber system extends the application of optical fiber technology beyond monitoring vibrations and temperatures in machine tools, offering a practical solution for enhancing surface integrity and manufacturing quality (Li et al., 2024; Tang et al., 2009).

EXPERIMENTAL SETUP

This study conducted precision surface grinding experiments on FC-300 gray cast iron, utilizing a dual-optical-fiber real-time measurement system to monitor strain and temperature variations of the workpiece under different machining conditions. The experimental setup primarily includes grinding equipment, workpiece material, optical fiber arrangement, and the data acquisition system.

Ultra-precision Surface Grinding Machine Experiment

To carry out ultra-precision grinding experiments on workpieces, the tooling machine used is a NAGASE-SGC630 ultra-precision surface grinding machine, whose accuracy can reach submicron, that is, $0.1 \mu m$. Hence, the processing plant needs to be in an environment with constant temperature and humidity and a cooling liquid for continuous cooling to keep the tooling machine in a good state of grinding. The workpiece is mainly placed horizontally on the machining platform, which is fixed by magnetic force, while the experimental instruments and fiber optic measuring instruments are placed on the table in front of the grinder. The grinder is operated to make the workpiece contact with the grinding wheel through the movement of the platform to carry out the grinding. Fig. 1. shows a picture of the workpiece placed on the grinder.



Figure 1. Workpiece placed on the grinding machine.

Workpiece Material

The workpieces used in this experiment were made of FC-300 gray cast iron, a material widely applied in the manufacturing of high-strength and high-rigidity components. Fig. 2. shows two pieces of gray cast iron (FC-300) prepared for grinding, with a size of about $100 \text{ mm} \times 70 \text{ mm} \times 20 \text{ mm}$, numbered A-2 and B-2.





Figure 2. Grinding of the gray cast iron to be tested (FC-300).

Experimental setup for workpiece measurement through a dual-fiber method

To assess the thermal strain, the thermal expansion coefficient of the FC-300 gray cast iron was measured using both an attached fiber and a free fiber. As illustrated in Fig. 3, the optical fiber was initially attached to the center of both the long and short sides of the workpiece. At each designated position, a free optical fiber was secured with thermal insulation tape to prevent it from being affected by strain. A thermocouple was positioned at the center of the fiber grating to monitor temperature changes. During the grinding process, the optical fiber was embedded within the material through a circular hole, with an additional thermocouple used to record temperature variations. Throughout the experiment, wavelength drift data from both the inner and side edges were collected, while the attached fiber was mounted on a horizontal platform for accurate measurements.

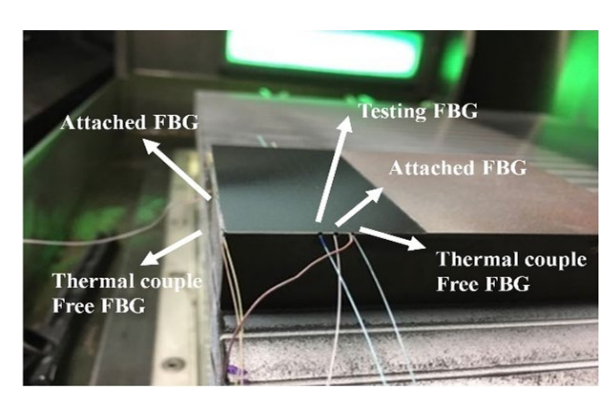


Figure 3. Illustration of the experimental setup for the dual-fiber method.

RESULTS AND DISCUSSION

Gray cast iron (FC-300) No. A-2 and B-2 workpieces are used to conduct 14 grinding experiments separately to discuss the temperature rise and strain data measured using the dual-fiber optic method for two types of workpieces.

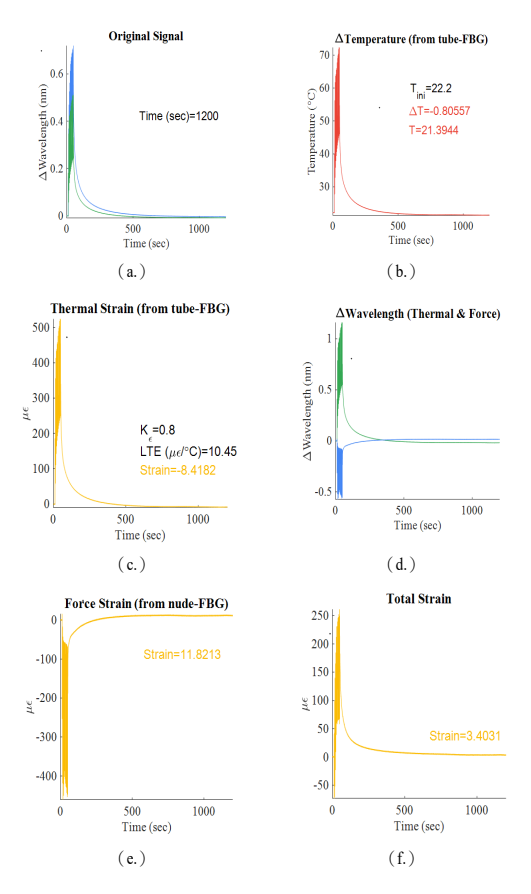


Figure 4. Internal measurement results of 14 grinding processes on No. A-2 workpiece.(Total:1200 s) (a.) Attached fiber & free fiber wavelength drift (b.) Temperature rise information (c.) Thermal stress information (d.) The wavelength drift of each of heat and force (e.) Force strain information (f.) Total strain information

No. A-2 Workpiece with 14 grinding passes

The machining process for No. A-2 workpiece includes 1200 rpm grinding wheel and 5000 mm/min feed rate for the 14 grinding experiments. Each grinding depth is 10 μ m, with a total grinding depth of 140 μ m. The sampling frequency for the experiment is set to 1000 Hz. Although the 14 grinding processes can be completed within 1 min, the experiment is conducted for 1200 s to allow the workpiece temperature to return to the initial temperature setting for measurement. Fig. 4. and Fig. 5. show the results of the measurement of the internal fiber group within 1200 s and the first 70 s of the machining process. Fig. 4. (a.) shows the wavelength drift of the two optical

fibers during the experiment, where blue is the attached optical fiber signal, and green is the free fiber signal.

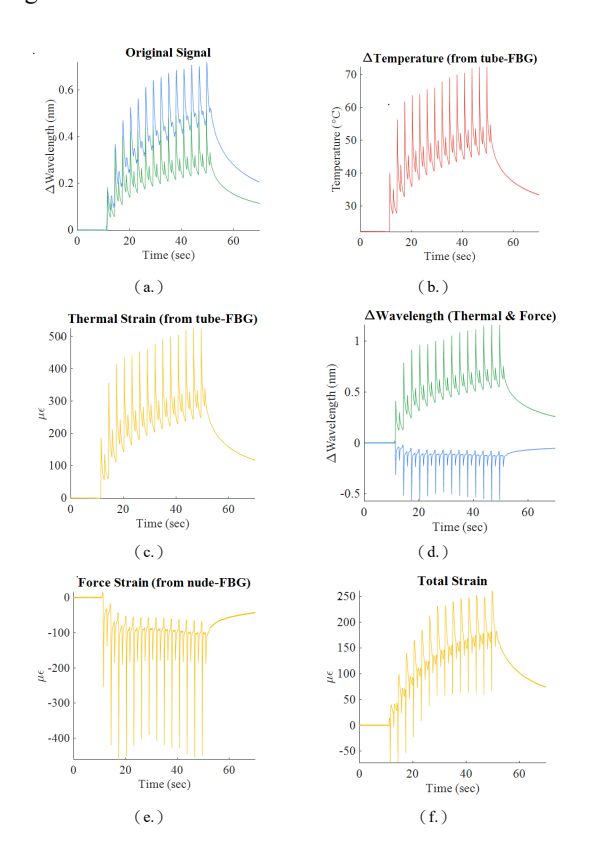


Figure 5. Internal measurement results of 14 grinding processes on No. A-2 workpiece) (first 70 s) (a.) Attached fiber & free fiber wavelength drift (b.) Temperature rise information (c.) Thermal stress information (d.) The wavelength drift of each of heat and force (e.) Force strain information (f.) Total strain information

The 28 contact signals of the 14 reciprocating grinds are measured on both optical fibers. Among the 14 grinding processes, the attached optical fiber wavelength only drifts about 0.7 nm, while the free optical fiber drifts about 0.2 nm. Fig. 4. (b.) demonstrates the measured temperature rise. After 14 grinding processes, the maximum internal temperature reaches about 70.00 °C. Fig. 4. (c.) is the result of free fiber temperature rise multiplied by the thermal expansion coefficient to deduce the thermal strain, where K ε =0.8. In the graph, the thermal strain is calculated by LTE=10.45, and the maximum thermal strain caused by the temperature rise in the cut is about 500με. In Fig. 4. (e.), the grinding process first causes compressive strain, with the maximum force strain causing a compressive strain of about -400 µE. At about 500 s, the strain shows a stable tensile strain with a value of about 11.82 με. Owing to the low grinding temperature, the grinding force exerts a minimal effect on the workpiece, forming a small tensile stress.

Therefore, the grinding temperature is speculated to be the main factor affecting residual strain.

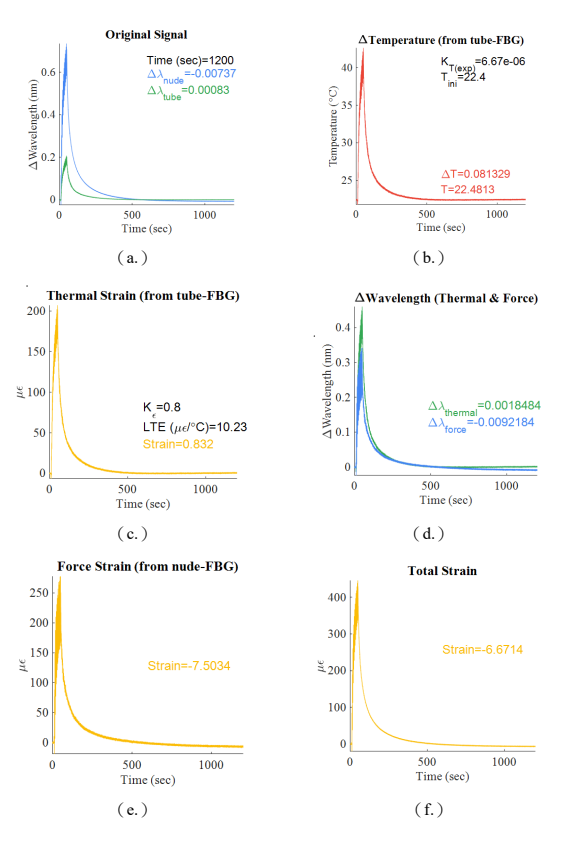


Figure 6. Side measurement results of 14 grinding passes on No. A-2 workpiece. (a.) Attached fiber & free fiber wavelength drift (b.) Temperature rise information (c.) Thermal stress information (d.) The wavelength drift of each of heat and force (e.) Force strain information (f.) Total strain information

Fig. 6. and Fig. 7. are under the same 14 grinding experiments. The temperature rise and strain information measured by the side optical fiber group refers to the information during the overall time and the first 70 s. Fig. 6. (a.) shows the signal of the original wavelength drift. The values measured by the optical fiber on the side are relatively lower than those measured inside. Given the far distance from the surface, the cutting force causes the signal to be relatively smooth. In Fig. 6. (b.), the temperature is only up to the maximum of about 43.00 °C. Fig. 6. (c.) presents that the maximum lateral thermal strain is about 200 $\mu\varepsilon$, and Fig. 6. (d.) indicates that during the grinding process on the side, the wavelength shift caused by the force is positive and quite close to the wavelength shift induced by heat. The strain of the force in Fig. 6. (e.) is only about $-7.5 \,\mu\varepsilon$ compressive strain at the end of the measurement. The residual strain measured inside and on the side of No. A-2 workpiece by the optical fiber is a small and negative compressive strain.

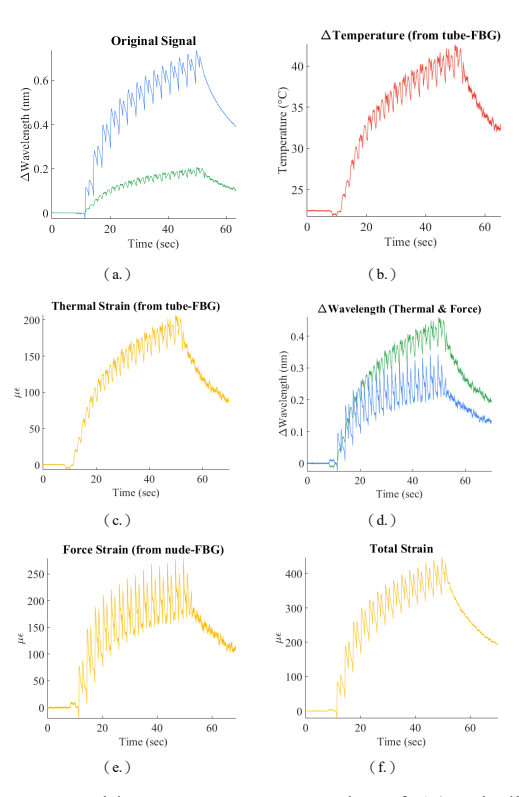


Figure 7. Side measurement results of 14 grinding passes on No. A-2 workpiece) (First 70 s) (a.) Attached fiber & free fiber wavelength drift (b.) Temperature rise information (c.) Thermal stress information (d.) The wavelength drift of each of heat and force (e.) Force strain information (f.) Total strain information

4.2 No. B-2 Workpiece with 14 grinding passes

After No. B-2 workpiece is fixed on the platform, the machining process is performed the same as that for No. A-2 workpiece. To allow the workpiece temperature to return to the initial temperature, the experiments are set to measure at the time of 1,000 s to carry out machining measurements. Fig. 8. shows the history of measured temperature rise, strain, and temperature reduction of the internal optical fiber in the 14 grinding processes. Fig. 8. (a.) is the wavelength drift situation during the experimental process, where blue is the attached optical fiber, and green is the free optical fiber. Because the main grinding is concentrated in the first 60 s, we can observe 2 nm drift for the attached optical fiber and 1 nm drift for the free optical fiber. At the end of grinding, the internal lattice structure of the workpiece is reorganized. The free optical fiber returns to the original wavelength drift at room temperature when the experimental time is about 400 s. After the temperature recovery, the attached optical fiber produces a negative wavelength drift due to the residual strain inside. Fig. 8. (b.) is the measured temperature rise of the free fiber, in which the temperature reaches 140°C during grinding, and the temperature at the end of the experiment is 22.78 °C. The temperature is only about 0.40 °C different from

the initial temperature, almost returning to room temperature.

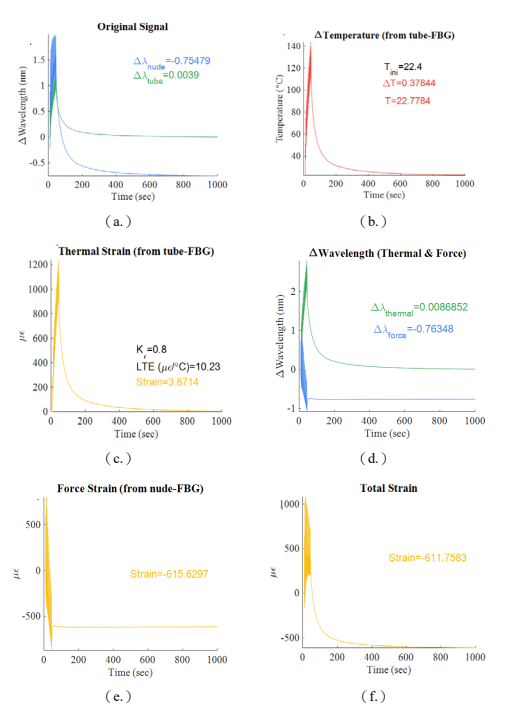


Figure 8. Internal measurement result of No. B-2workpiece) from 14 grinding processes. (a.) Attached fiber & free fiber wavelength drift (b.) Temperature rise information (c.) Thermal stress information (d.) The wavelength drift of each of heat and force (e.) Force strain information (f.) Total strain information

Fig. 8. (c.) is the result of free fiber temperature rise multiplied by the thermal expansion coefficient to deduce the thermal strain, where K ε =0.8, and LTE=10.23. The maximum thermal strain caused by the temperature rise in the cut is about 1200 µε. As the temperature returns to the initial temperature, the thermal strain is finally about 3.87 µE. Fig. 8. (d.) shows the wavelength drift caused by heat and force after decoupling, with green representing the wavelength drift induced by heat, which includes temperature rise and thermal strain. High temperatures cause a drift of about 2 nm in heat, and as the temperature drops to the starting temperature, the wavelength drift of the green line also returns to the initial value. The blue line represents the wavelength drift caused by force. The grinding force induces residual strain in the internal lattice structure of the material, with the residual wavelength drift being about -0.76 nm. Fig. 8. (e.) is the analyzed force strain, which contains the strain caused by the cutting force and the temperature drop in the lattice reorganization. The strain value becomes a certain value after 70 s of the grinding process, that is, about $-615.63 \mu\epsilon$. Fig. 8. (f.) is the total strain, including thermal and force strains. After 70 s, residual strain is gradually formed inside the material.

The final strain value is a compressive residual strain of approximately $-611.76 \,\mu\text{E}$, which is mainly caused by strain and stress strain other than the temperature rise of force and lattice reorganization.

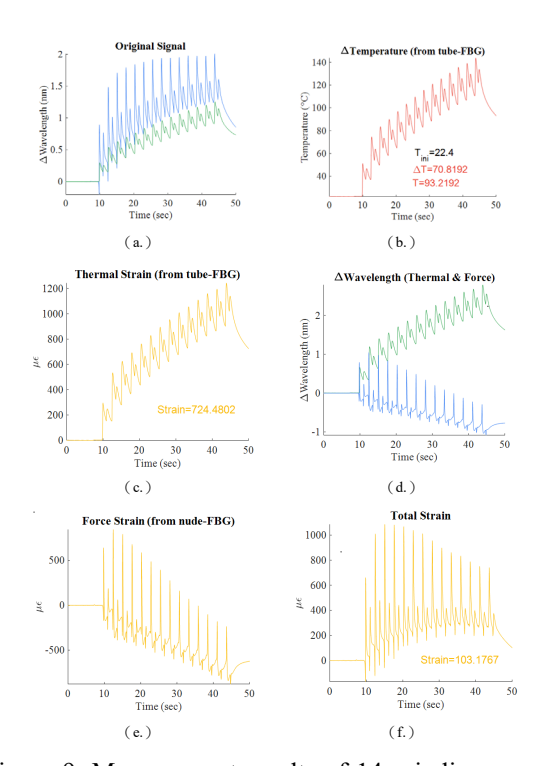


Figure 9. Measurement results of 14 grinding passes of No. B-2 workpiece (zoomed in to the first 50 s) (a.) Attached fiber & free fiber wavelength drift (b.) Temperature rise information (c.) Thermal stress information (d.) The wavelength drift of each of heat and force (e.) Force strain information (f.) Total strain information

Fig. 9. is the process of the same experiment with the time axis zoomed in to the first 50 s, in which the high-resolution characteristics of the fiber Bragg grating detailedly record the information of the brief grinding process. In Fig. 9. (a.), the values measured by the attached fiber are higher than those by the free fiber. The attached fiber is subject to force strain, making the signal of the attached fiber sharper than that of the free fiber. Because the grinding wheel reciprocates back and forth for one pass, both fibers measure a small peak value under the main peak value. which is the grinding signal during the reciprocating recovery. Fig. 9. (b.) shows the temperature rise signal during the grinding process. In the same pass, the grinding wheel reciprocates back and forth over the surface, with each main pass causing the workpiece to rise by about 20.00 °C. The temperature rise from the recovery grinding after the main pass is also measured, with the workpiece ultimately reaching about 140.00 °C. The detailed information marked in the figures in this paper, such as the red labels Δ "T=70.8192" and "T=93.2192" in this figure, indicates the analysis

results at the end of the time axis of the figures; in this figure, it is the temperature rise from 0 s to 50 s. Fig. 9. (c.) depicts the thermal strain of the workpiece during the grinding process, which follows the same trend as the temperature rise. Fig. 9. (d.) shows the force and thermal wavelength drift during the grinding process; the instantaneous cutting force pulling on the grating results in the blue force wavelength drift signal being sharper than the green thermal wavelength drift signal. Fig. 9. (e.) demonstrates the resolved force strain. In each grinding pass, the grinding wheel produces a positive strain on the workpiece, after which the internal structure begins to reorganize, gradually forming a compressive residual strain. Fig. 9. (f.) shows the total strain for the first 50 s. Given that the temperature rise effect is still present, the total strain is mainly dominated by the tensile strain of the thermal strain.

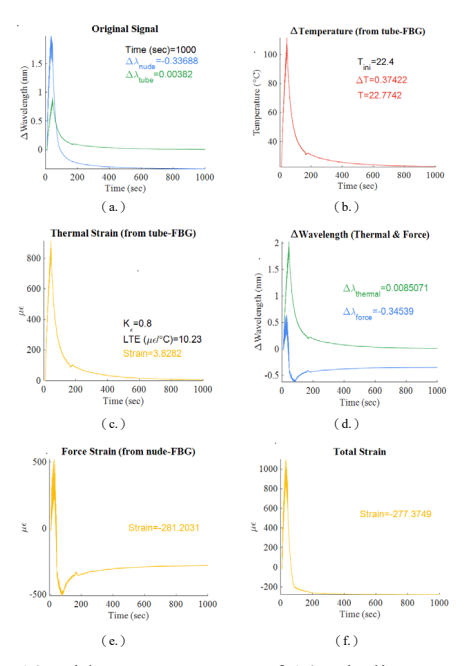


Figure 10. Side measurement of 14 grinding passes of No. B-2 workpiece. (a.) Attached fiber & free fiber wavelength drift (b.) Temperature rise information (c.)Thermal stress information (d.) The wavelength drift of each of heat and force (e.) Force strain information (f.) Total strain information

Fig. 10. and 11. show the overall result and the results in the first 60 s of the same experiment with 14 grinding passes, with the temperature rise and strain measured by the side optical fiber. Fig. 10. (a.) presents the wavelength drift during the experiment. Because they are not as close to the surface as the internal fiber, the peak signal waveforms of the attached and free fibers are relatively smoother, but the 28 peaks within the 14 cuts can be distinctly measured. Fig. 10. (b.) shows the temperature rise of the workpiece, which reaches about 120°C during grinding, that is, about 20 °C less than that of the

internal fiber. Fig. 10. (c.) illustrates the thermal strain during the grinding process; owing to the small temperature rise, the maximum thermal strain is about 900 $\mu\varepsilon$. Fig. 10. (d.) shows the wavelength drift due to force and heat separately; the force wavelength drift starts as a positive value at the beginning of cutting and gradually forms a negative value of compressive strain after subsequent cuts. Around 200 s, a small spike due to occasional data loss from the wavelength demodulator occurs, speculated to be caused by a decrease in light energy, which does not affect the measurement. Fig. 10. (e.) exhibits the history of force strain. After the grinding is completed, the workpiece gradually forms a compressive strain. Around 400 s, a fixed value of residual strain is formed, with a value of about $-281.20 \,\mu\varepsilon$.

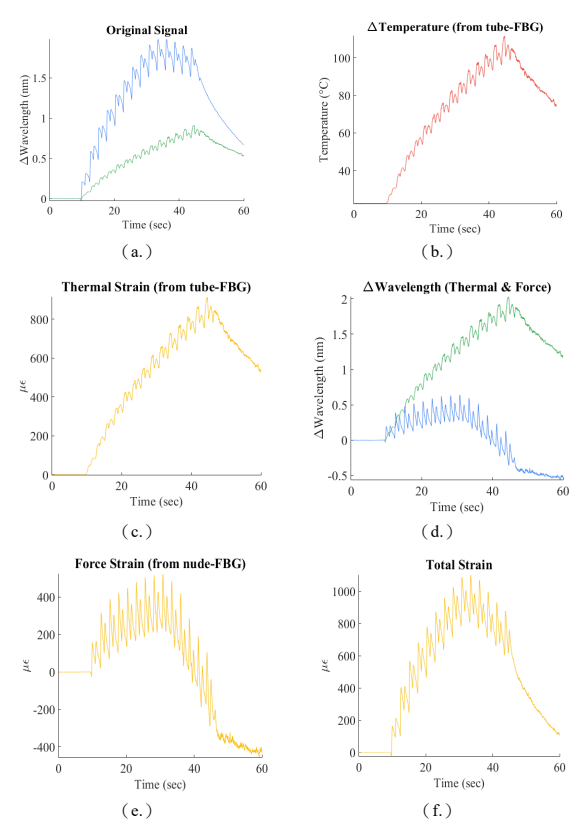


Figure 11. Flank measurement of No. B-2 workpiece of 14 grinding passes (first 60 s) (a.) Attached fiber & free fiber wavelength drift (b.) Temperature rise information (c.) Thermal stress information (d.) The wavelength drift of each of heat and force (e.) Force strain information (f.) Total strain information

Fig. 10. (f.) shows the total strain added up, subtracting the residual thermal strain, with a residual compressive strain of about $-273.00~\mu\varepsilon$ on the side position. Because the side is deep and far from the machining surface, the final value is a compressive strain internally and on the side, with quantitative differences depending on the depth position.

In the grinding experiment, the temperature

information is mainly converted by the optical fiber. To verify that the measured temperature information is accurate, the temperature rise measured in a cutting experiment is compared with that measured using a thermocouple. Fig. 12. and Fig. 13. are the comparisons of the internal and side temperatures, where the red color is the thermocouple temperature rise information, and the black color is the internal temperature rise information measured by the optical fiber. Given that the sampling frequency of the thermocouple is only 2 Hz, its fluctuation amplitude is obviously larger than that of the fiber optics, which has a very high sampling rate. In terms of measurement values, owing to the high resolution of the optical fiber, the whole processing details can be shown. Although the thermocouple can only roughly see the trend of temperature rise, the two measurements are quite consistent with the temperature, which confirms the ability of the fiber optic gratings to measure temperature rise.

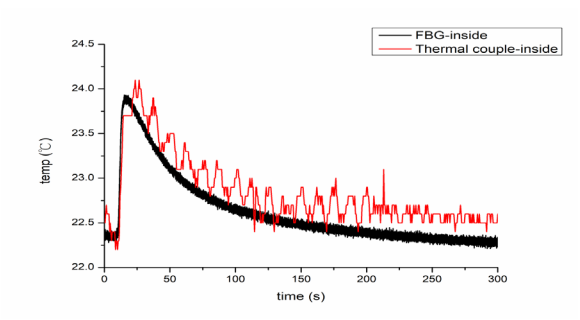


Figure 12. Comparison of the internal temperature rise of No. B-2 workpiece

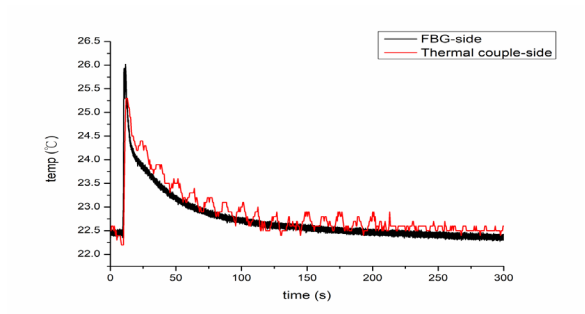


Figure 13. Comparison of temperature rise on the side of No. B-2 workpiece.

CONCLUSIONS

This study presents a groundbreaking dual-fiber real-time measurement system designed to analyze internal residual stress in grinding processes. By embedding high-sensitivity optical fibers in the workpiece, the system enables real-time measurement of internal strain under various grinding conditions. This novel approach addresses the limitations of traditional methods, providing a non-destructive, cost-effective, and immediate analysis of thermal stress and

residual strains.

Experimental results validate the system's effectiveness, showing a clear correlation between cutting depth and workpiece temperature, with normal grinding conditions primarily causing pressure deformation and residual compression strain. The system's ability to decouple strain caused by force and heat through resonant wavelength wander theory enhances its precision and reliability. Lower temperature cutting and grinding wheel dressing were found to mitigate residual strain, highlighting practical strategies for improving grinding outcomes.

The findings from fourteen grinding experiments on gray cast iron (FC-300) workpieces demonstrate the system's potential for industrial application, with the maximum thermal and force strains providing crucial insights into the grinding process. This innovative measurement system not only advances the understanding of residual stress formation but also offers a valuable tool for optimizing grinding techniques, ultimately contributing to enhanced surface integrity and component performance in manufacturing.

DISCLOSURE STATEMENT

The list of authors and the corresponding authors' names follow the telephone communication with Chien-Ching Ma on 03/06/2024.

REFERENCES

Shuto, Y., Yanagi, S., Asakawa, S., Kobayashi, M., and Nagase, R., "Fiber fuse phenomenon in step-index single-mode optical fibers," *IEEE Journal of Quantum Electronics*, vol. 40, no. 8, pp. 1113-1121 (2004).

Sanchez-Pérez, J.F., Solano-Ramírez, J., Marín-García, F., and Castro, E., "A Study Using the Network Simulation Method and Nondimensionalization of the Fiber Fuse Effect," *Axioms*, vol. 14, no. 2, pp. 1-17 (2025).

Breidenstein, B., Vogel, N., and Bergmann, B., "Influence of the preparation processes on the residual stresses in PCD and PcBN tools," *European Journal of Materials*, vol. 4, no. 1, pp. 2350936 (2024).

Li, X., Liu, J., Wu, H., Miao, K., Wu, H., Li, R., Liu, C., Fang, W., and Fan, G., "Research progress of residual stress measurement methods," *Heliyon*, vol. 10, e28348 (2024).

Zhang, J., Meng, X., Du, J., Xiao, G., Chen, Z., Yi, M., and Xu, C., "Modelling and Prediction of Cutting Temperature in the Machining of H13 Hard Steel of Transient Heat Conduction," *Materials*, vol. 14, no. 3176, pp. 1-12 (2021).

Hadad, M., and Sadeghi, B., "Thermal analysis of minimum quantity lubrication (MQL) grinding process," *International Journal of*

- Machine Tools and Manufacture, vol. 63, pp. 1-15 (2012).
- Grigoriev, S.N., Starkov, V.K., Gorin, N.A., Krajnik, P., and Kopac, J., "Creep-Feed Grinding: An Overview of Kinematics, Parameters and Effects on Process Efficiency," *Strojniški vestnik Journal of Mechanical Engineering*, vol. 60, no. 4, pp. 213-220 (2014).
- Qian, N., Jamil, M., Ding, W., Fu, Y., and Xu, J.,
 "Thermal management in grinding of
 superalloys A critical review," *Journal of Intelligent Manufacturing and Special Equipment*, vol. 5, no. 1, pp. 3-33 (2024).
- Gostimirovic, M., Madic, M., Sekulic, M., Rodic, D., and Aleksic, A., "A gradient-based optimal control problem in creep-feed grinding," *The International Journal of Advanced Manufacturing Technology*, vol. 121, pp. 4777–4791 (2022).
- Storchak, M., Stehle, T., and Möhring, H.-C., "Numerical Modeling of Cutting Characteristics during Short Hole Drilling: Part 2—Modeling of Thermal Characteristics," *Journal of Manufacturing and Materials Processing*, vol. 8, no. 1, p. 13 (2024).
- Rowe, W.B., "Basic Material Removal," in *Principles* of Modern Grinding Technology (Second Edition), Oxford: William Andrew Publishing, pp. 15-33 (2014).
- Lyu, Y., Wang, G., Li, X., Shu, Q., and Wang, B., "A strategy of hob-grinding the cylindrical riblet surface for drag reduction by the grinding wheel with ordered abrasive pattern," *The International Journal of Advanced Manufacturing Technology*, vol. 134, pp. 5973–5984 (2024).
- Li, B., Li, X., Hou, S., Yang, S., Li, Z., Qian, J., and He, Z., "Prediction and analysis of grinding force on grinding heads based on grain measurement statistics and single-grain grinding simulation," *The International Journal of Advanced Manufacturing Technology*, vol. 132, pp. 513–532 (2024).
- Tang, J., Du, J., and Chen, Y., "Modeling and experimental study of grinding forces in surface grinding," ASME Journal of Manufacturing Science and Engineering (2009).